Differential growth and shape formation in plant organs

Changjin Huang[a,1], Zilu Wang[b], David Quinn[b], Subra Suresh[c,2], and K. Jimmy Hsia[a,b,d,e,2]

[a]Department of Biomedical Engineering, Carnegie Mellon University, Pittsburgh, PA 15213; [b]Department of Mechanical Engineering, Carnegie Mellon University, Pittsburgh, PA 15213; [c]Nanyang Technological University, 639798 Singapore, Republic of Singapore; [d]School of Mechanical and Aerospace Engineering, Nanyang Technological University, 639798 Singapore, Republic of Singapore; and [e]School of Chemical and Biomedical Engineering, Nanyang Technological University, 639798 Singapore, Republic of Singapore

Contributed by Subra Suresh, October 14, 2018 (sent for review July 2, 2018; reviewed by Markus J. Buehler and Huajian Gao)

Morphogenesis is a phenomenon by which a wide variety of functional organs are formed in biological systems. In plants, morphogenesis is primarily driven by differential growth of tissues. Much effort has been devoted to identifying the role of genetic and biomolecular pathways in regulating cell division and cell expansion and in influencing shape formation in plant organs. However, general principles dictating how differential growth controls the formation of complex 3D shapes in plant leaves and flower petals remain largely unknown. Through quantitative measurements on live plant organs and detailed finite-element simulations, we show how the morphology of a growing leaf is determined by both the maximum value and the spatial distribution of growth strain. With this understanding, we develop a broad scientific framework for a morphological phase diagram that is capable of rationalizing four configurations commonly found in plant organs: twisting, helical twisting, saddle bending, and edge waving. We demonstrate the robustness of these findings and analyses by recourse to synthetic reproduction of all four configurations using controlled polymerization of a hydrogel. Our study points to potential approaches to innovative geometrical design and actuation in such applications as building architecture, soft robotics and flexible electronics.

morphogenesis | growth | soft matter | 3D structure

Biological systems have developed versatile design strategies through evolution over billions of years. Uncovering these design principles not only elucidates the mechanisms underlying the evolution of living systems, but also establishes the scientific basis for biomimetics whereby advanced materials and systems could be developed based on lessons learned from nature. Examples of plant-inspired engineering systems include: superhydrophobic surfaces designed with strategies drawn from the structure of the lotus leaf (1); self-repairing antifouling surfaces inspired by the pitcher plant (2); and actuation systems inspired by the Venus flytrap (3–5). Motivated by the wide variety and diversity of 3D shapes of plant organs, much effort has been devoted to identifying the genetic and biomolecular pathways that regulate cell division and/or cell expansion as well as shape formation (6–9). Although specific genes dictate cell growth in a programmed manner, biomechanics also plays an essential and significant role in the formation of 3D shapes at the organ level. Compositional inhomogeneity of the constituent materials or the polarized intercellular transport of growth factors leads to inhomogeneous and nonuniform growth in various parts of plant organs such as leaf, stem, root, flower, and fruit and, consequently, leads to mismatch of growth strain (10, 11). In contrast to mammalian cells which can migrate to accommodate the need for extra spaces, the physical constraints in adjoining plant cell walls force adjacent cells to deform in a coordinated manner, facilitating the emergence of complex shapes (12–16).

A leaf blade or a flower petal mainly consists of two layers of mesophyll cells sandwiched between two layers of epidermis, with vascular veins lying in the median plane of the mesophyll. Differential cell expansion between the upper and lower sides of the mesophyll in response to environmental stimuli (e.g., temperature, light, or humidity) is responsible for the repeated opening and closure of the flower (17). However, excessive cell growth within the marginal region plays a dominant role in the formation of saddle shapes and rippled edges in leaves and flower petals that open only once (18, 19). Besides saddle shapes and localized ripples, helical growth represents another growth pattern commonly seen in nature (20). Direct correlation between the helical growth of stems and the helical pattern of microtubules has also been observed (21, 22). In addition, cell wall composition could dictate the helical growth of plant cells (23). Our current state of understanding of the mechanisms of morphogenesis and shape evolution in plant organs is not sufficiently complete to conclude whether the observed helical pattern of microtubules or cells is the cause or consequence of the helical growth of the organ. In addition, the seemingly random evolution of twisting directions in some species points to the possibility of nongenetic factors influencing the emergence of helical growth of plant organs (20).

In this study, we investigate the origins of 3D shapes driven by biomechanical constraints and differential growth in plant organs

Significance

Plant leaves and flower petals in nature exhibit a wide variety of complex 3D shapes. Formation of these shapes has largely been studied from genetic and biomolecular viewpoints, overlooking contributions from biophysical factors such as mechanical stress and deformation. By means of computational simulations and quantitative analyses of the growth strains in live plant organs, we develop fundamental mechanistic insights into how nature invokes mechanics in the evolution of four commonly found shapes in plant organs by differential growth. We also demonstrate how these common shapes can be synthetically reproduced in hydrogel using this mechanistic understanding. Our study provides a broad scientific framework for rationalizing plant organ morphogenesis, but also provides pathways for generating bioinspired 3D architectures in soft materials.

Author contributions: D.Q., S.S., and K.J.H. designed research; C.H. and Z.W. performed research; C.H., Z.W., S.S., and K.J.H. analyzed data; and C.H., S.S., and K.J.H. wrote the paper.

Reviewers: M.J.B., Massachusetts Institute of Technology; and H.G., Brown University.

Conflict of interest statement: C.H., S.S., and K.J.H. have filed for invention disclosure based on the work presented in this paper.

[1]Present addresses: School of Mechanical and Aerospace Engineering and School of Chemical and Biomedical Engineering, Nanyang Technological University, 639798 Singapore, Republic of Singapore.

[2]To whom correspondence may be addressed. Email: ssuresh@ntu.edu.sg or kjhsia@ntu.edu.sg.

This article contains supporting information online at www.pnas.org/lookup/suppl/doi:10.1073/pnas.1811296115/-/DCSupplemental.

Published online November 19, 2018.

by recourse to quantitative experiments on live plant organs and detailed finite element simulations. On this basis, we present here a scientific framework that establishes a morphological phase diagram which is capable of rationalizing four geometric configurations commonly found in plant organs: twisting, helical twisting, saddle bending, and edge waving. Our results show that the morphology of a growing leaf is determined by both the maximum value and the spatial distribution of growth strain. We further demonstrate the robustness of our scientific findings on differential growth-induced morphogenesis by synthetic reproduction of all four common geometric configurations in our phase diagram in a model hydrogel system that mimics plant growth through controlled manipulation of the polymerization process. Our study thus not only provides a broad framework for elucidating the evolution of plant physiology, but also points to potential approaches for innovative geometrical design and actuation in such applications as building architecture, soft robotics, and flexible electronics.

Results

Three-Dimensional Shapes of Long Plant Leaves and Flower Petals. An elevated growth factor level within the marginal region of plant leaves or flower petals often results in an excessive local growth rate and a mismatch of growth strain. The accumulated residual stresses eventually facilitate out-of-plane deformation instability, leading to a large variety of 3D shapes in nature. Fig. 1*A* shows images of four representative 3D shapes of long orchid petals, from which we identify the corresponding four basic configurations. Configuration I shows the twisting growth of long petals of *dendrobium helix*, whose centers remain approximately straight from the base to the distal end. In contrast, the petals of *prosthechea cochleata* exhibit a helical twisting morphology (Configuration II) where the petals' centers follow a helical pattern. The petals of *brassavola nodosa* bend into a saddle shape (Configuration III) whose two principal curvatures feature opposite signs. The long petals of *phragmipedium brasiliense* feature wavy patterns along petal margins (Configuration IV). More complex petal morphologies resulting from the combination of these configurations are also present in nature (*SI Appendix*, Fig. S1).

The central question for this study is, how does the differential growth in these leaves influence their morphogenesis? We collected live leaves from several species (from the Phipps Conservatory and Botanical Garden in Pittsburgh, PA). To quantify the growth strain profile of a leaf, we dissected them into individual narrow strips parallel to the stem and measured the length of each strip, as illustrated in Fig. 1 *B* and *C*. We observed that dissecting half of the leaf leads to a change in the shape of the other half, suggesting the existence of residual stresses in its natural state. We define the growth strain as $\varepsilon_g = (l - l_0)/l_0$, where l_0 and l are the lengths of the center stem and the strip at a distance y from the stem, respectively. As shown in Fig. 2*A*, the growth strain profiles along the width direction can be approximated by a power-law function, as

$$\varepsilon_g(y) = \beta\left(\frac{y}{W}\right)^n, \qquad [1]$$

where y and W are the distance from the strip to the center and half-width of the leaf, respectively. The growth strain monotonically increases from zero at the center to a maximum value, β, at the edge when $y = W$. The power-law exponent, n, characterizes the steepness of the differential growth strain profile. Fig. 2*B* shows that the leaves with a twisting configuration feature a parabolic growth strain profile ($n \sim 2$), and those with edge-waving configuration feature a steeper increase in growth strain near the marginal region, leading to a higher n value. Compared with leaves with twisting or edge-waving configuration, leaves

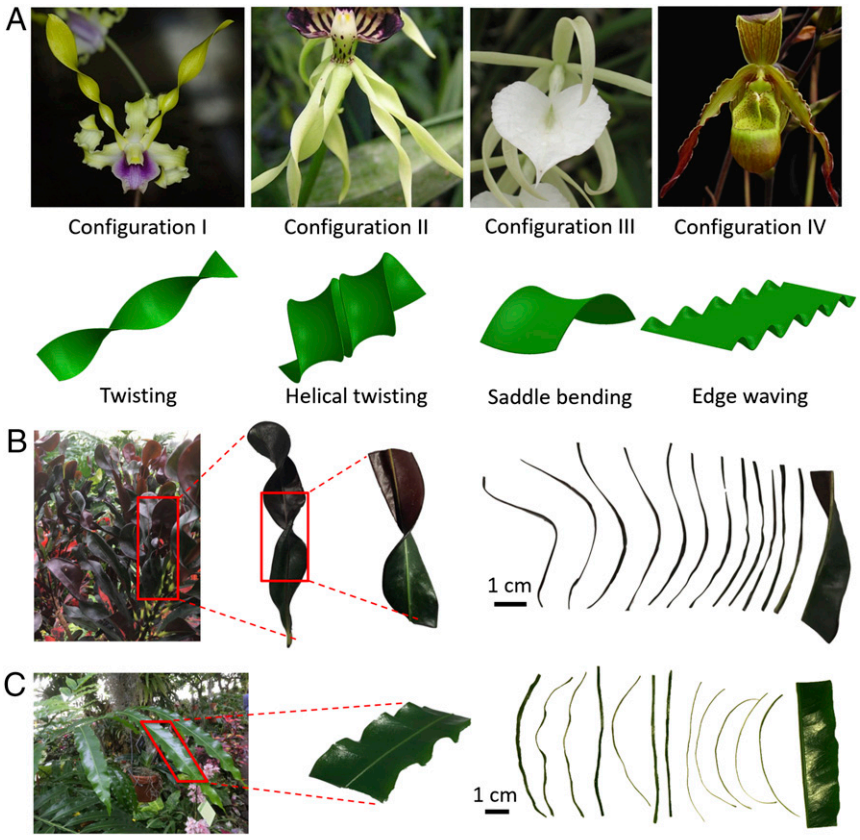

Fig. 1. Observations and experiments on live plant leaves. (*A*) Three-dimensional morphologies of long orchid petals (images from www.speciesorchids.com/CeretobeDendrobiums.html; https://queenslandorchid.files.wordpress.com/2014/03/prosthechea-cochleata.jpg; https://commons.wikimedia.org/wiki/File:Brassavola_nodosa_-_Flicker_003.jpg; and https://www.orchidweb.com/orchids/phragmipedium/species/phrag-brasiliense-clone-a) with the corresponding basic buckling configurations. From *Left* to *Right*: *d. helix* in twisting (Configuration I), *p. cochleata* in helical twisting (Configuration II), *b. nodosa* in saddle bending (Configuration III), and *phragmipedium brasiliense* in edge waving (Configuration IV). Configuration I image courtesy of Paul Zorn (photographer). Configuration II image courtesy of SoundEagle/Queensland Orchids International. Configuration III image courtesy of Wikimedia Commons/Elena Gaillard. Configuration IV image courtesy of Orchids Limited. (*B* and *C*) Dissection of twisting croton mammy (*codiaeum variegatum*) leaf (*B*) and edge-waving fern tree (*filicium decipiens*) leaf (*C*) into thin strips for growth strain quantification.

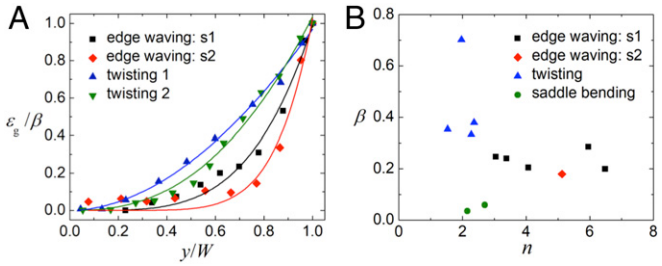

Fig. 2. Quantitative experimental characterization of growth strain profile of live plant leaves. (*A*) Representative growth strain profiles of leaves with twisting- and edge-waving configurations normalized by maximum growth strain. (*B*) Plot of n- and β-values of twisting, edge-waving, and saddle-bending leaves. Leaves with edge-waving configuration are taken from two different species: fern tree (*filicium decipiens*; edge waving: *B, s1*) and croton "interruptum" (*c. variegatum*; edge waving: *B, s2*).

with saddle-bending configuration feature much smaller maximum growth strain level ($\beta < 0.1$).

Mechanistic Modeling of a Growing Leaf. To investigate the effect of growth strain on morphogenesis, we conducted finite-element method (FEM) simulations of a long rectangular leaf with a nonuniform growth strain across its width direction (Fig. 3*A*). The growth strain increases from zero at the center to the maximum value at the edge. As shown in Fig. 3*B*, increasing the value of n increases the steepness of the strain profile near the leaf margin and reduces the steepness of the strain profile in the interior region. In the present FEM simulations, we modeled the growth process as an equivalent thermal expansion problem. We allow the leaf to grow only along the x-axis direction by prescribing a uniform nonzero thermal expansion coefficient but a nonuniform temperature field, while expansion along the other directions is prevented via a vanished thermal expansion coefficient. The temperature field, in a stress-free state, leads to a strain field which is the same as the growth strain distribution in Eq. **1**.

In all simulations, deformation commences as planar at small growth strain, and instability then occurs at a critical level. Like many thin-film systems under constraint, the resulting buckled configuration is dictated by local strain fields (24–26). Here, the two critical parameters controlling the shapes of buckled configurations are β and n, which for thin plant organs are dependent on species and age. Therefore, they can vary over a large range (Fig. 2*B*). Although plant cells exhibit viscoelastic properties in stretch tests (27), we modeled the growing petal as an elastic material for the following reasons. First, the mechanical response of plant cells is captured by a standard linear solid material model (i.e., two Maxwell elements in parallel with an elastic spring), with a characteristic time of relaxation on the order of seconds (28). However, the complete morphogenesis process of a growing leaf occurs over a time scale of several days. Because morphogenesis is primarily driven by cell proliferation and cell growth, growth strain dominates total deformation of the growing petal. Young's modulus and Poisson ratio values were set at $E = 350$ MPa and $\nu = 0.25$, respectively (27). We considered a full range of exponent n and maximum strain β. Fig. 3 highlights the results for $n = 2$ and $n = 10$.

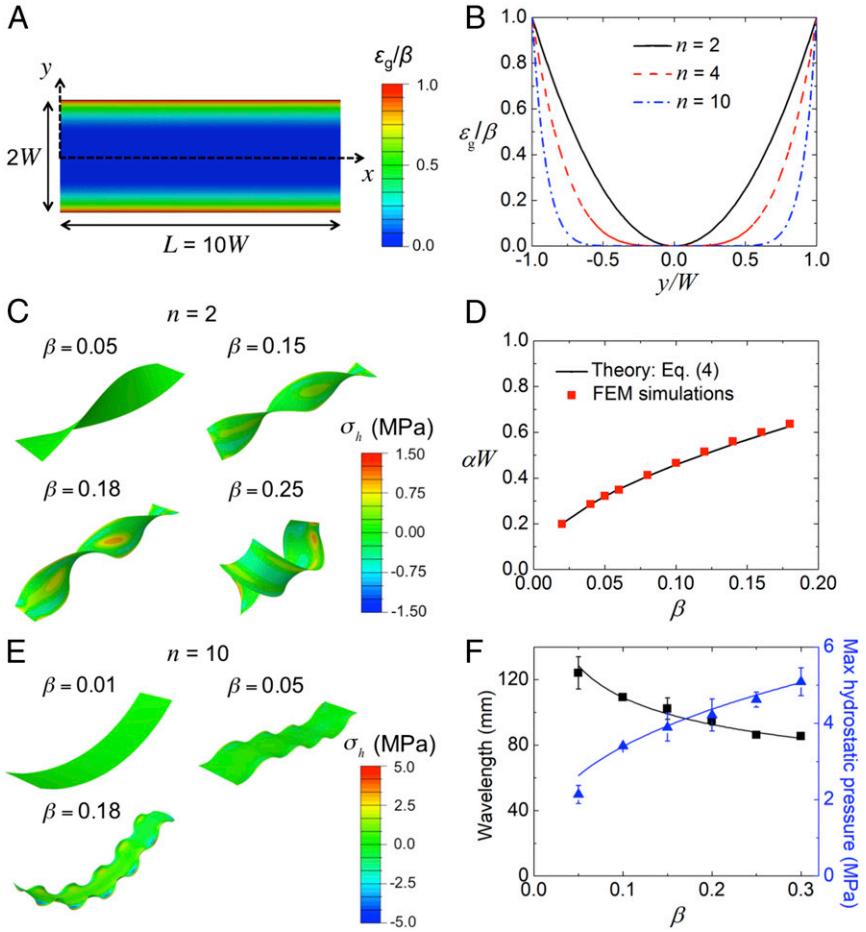

Fig. 3. FEM of a growing leaf. (*A*) Representative growth strain distribution normalized by maximum growth strain at the edge within a long leaf (strain increases from center to edge, but remains uniform along length direction). (*B*) Differential growth strain profiles with various n values normalized by the maximum growth strain. (*C*) Emergence of twisting- and helical-twisting configurations at $n = 2$. Contours of hydrostatic stress at various maximum strain levels are plotted. (*D*) Normalized twist angle per unit length as a function of the maximum strain at $n = 2$. The theoretical prediction is from Eq. **4**, and the simulation results are from FEM. (*E*) Emergence of saddle-bending and edge-waving configurations at $n = 10$. Color contours of hydrostatic stress at various maximum strain levels are plotted. (*F*) Wavelength of the edge waves and maximum hydrostatic stress level as a function of the maximum strain at $n = 10$.

For parabolic growth strain distribution with $n = 2$, the first instability consistently leads to twisting (Configuration I) at an intermediate maximum growth strain level ($\beta \sim 0.15$), representing the onset of initial instability from planar to 3D mode (Fig. 3*C*). *SI Appendix*, Fig. S2*A* shows the total strain energy stored in the leaf as a function of maximum strain. As expected, when the strain is low, the total strain energy increase scales with the square of strain, featuring a slope of $m = 2.0$ in the log–log plot. Initiation of instability is clearly captured by a sudden change in the slope, from quadratic to a nearly linear dependence of $m = 1.0$ (see *SI Appendix* for theory). As shown in Fig. 3*C* and *SI Appendix*, Fig. S3, a twisted configuration at a low growth strain level is nearly stress-free. Solely from geometric considerations, we note that shape change of a leaf from stress-free planar into stress-free twisting configurations requires a growth strain profile given by

$$\varepsilon_g(y) = \sqrt{1 + (\alpha y)^2} - 1, \qquad [2]$$

where α is the twist angle per unit length along the stem. Taylor expansion of Eq. **2** gives

$$\varepsilon_g(y) = \frac{1}{2}(\alpha y)^2 - \frac{1}{8}(\alpha y)^4 + \frac{1}{16}(\alpha y)^6 + \cdots \approx \frac{1}{2}\alpha^2 W^2 \left(\frac{y}{W}\right)^2, \qquad [3]$$

when the fourth-order term is one order of magnitude smaller than the second-order term, the maximum strain at edge $\beta = (1/2)\alpha^2 W^2 \leq 0.2$. Eq. **3** indicates that, at a low maximum strain level ($\beta \leq 0.2$), the formation of twisting configuration is energetically favorable for $n = 2$. The twisting angle per unit length as a function of the maximum growth strain is derived from Eq. **2** as

$$\alpha = \frac{\sqrt{2\beta + \beta^2}}{W}. \qquad [4]$$

Fig. 3*D* shows that α increases monotonically with increasing strain. Results from the FEM simulations are in good agreement with theoretical prediction. At a fixed maximum growth strain, wider leaves or petals twist less than narrower ones.

Interestingly, at a low maximum growth strain level ($\beta \sim 0.05$), both twisting and saddle-bending configurations emerge as two local energy minimum states. Careful energetic analysis shows that the strain energy of the saddle-bending configuration is relatively lower than that of the twisting configuration, but the relative energy difference between these two configurations is less than 10% (*SI Appendix*, Fig. S4). Fig. 3*C* shows that, as growth strain increases ($\beta > 0.15$), residual stresses due to in-plane stretch gradually build up as higher-order terms in Eq. **3** become more important. Thus, maintaining the twisting configuration becomes energetically more unfavorable. Consistent with the theory, our simulations reveal a transition from twisting to helical twisting (Configurations II) when the maximum growth strain approaches a critical level around $\beta = 0.2$. This transition occurs with the deviation of center axis away from a straight line and a nonuniform distribution of the von Mises effective stress (*SI Appendix*, Fig. S3). A sudden release (drop) of total strain energy is observed as a result of the mode transition, as clearly shown in *SI Appendix*, Fig. S2*B*.

For steeper change of growth strain, $n = 10$ (Fig. 3*B*), saddle-bending configurations become energetically more favorable than twisting, as shown in Fig. 3*E*. This is mainly due to the fact that differential growth predominately concentrates in the marginal region of the leaf at higher n values. Consequently, twisting introduces significant in-plane stresses and high strain energy in the interior region. At low growth strains, the leaf grows into a saddle shape (Configuration III). Further increase in growth strain leads to the emergence of an undulating wavy pattern. Eventually, competition between bending in the marginal region and stretching in the interior results in edge waving (Configuration IV). Our simulation (Fig. 3*F*) shows that the wavelength of edge waves decreases with increasing maximum strain level and follows a power-law relationship of $\lambda \sim \beta^{-0.2}$. The stress contours in Fig. 3*E* show that the highest hydrostatic stress levels occur at the peaks and valleys of the edge waves, and that hydrostatic pressure increases with an increase in maximum growth strain. Considering that hydrostatic pressure may alter normal nutrient and growth factor transport and/or cell wall remodeling needed for growth (29–31), the increase in pressure level is expected to influence the leaf's morphogenesis.

Through parametric simulations we developed a phase diagram of the morphogenesis of a growing leaf. Fig. 4 shows the parameter space (n, β) of different morphogenesis configurations (I, II, III, and IV). The experimental results measured from live leaves (Fig. 2*B*) are superposed as data points on the phase diagram. Note that the boundaries between different zones are approximate. In particular, between the saddle-bending (Configuration III) and edge-waving (Configuration IV) regions, simulations show a wide transition zone featuring configurations with kinks along the length direction but without regular periodic waves along edges. The emergence of a kink from the saddle-bending configuration is a result of a structural instability, accompanied by release of residual stresses in the central region, and by sudden strain energy drop as shown in *SI Appendix*, Fig. S2*D*. At higher maximum strain β and higher n values, however, this kink transition zone gives way to the edge-waving zone (Fig. 4).

Although the general trend of the simulation-generated phase diagram is consistent with the measurements from live leaves, there are some apparent discrepancies in the details. Our simulations predict that a twisting leaf transits into a helical twisting configuration when $\beta \approx 0.2$. However, measurements from twisting croton "mammy" leaves show that this transition occurs at higher maximum growth strains (one leaf even has a maximum strain of $\beta \approx 0.7$, Fig. 2*B*). This apparent discrepancy can readily be rationalized through considerations of a stiff midvein in croton mammy leaves. As shown in Fig. 3*C*, change from twisting to helical twisting requires bending of the centerline, thus a higher driving force for a stiff midvein. Therefore, the twisting-to-helical twisting transition is expected to occur at a much larger maximum growth strain in the presence of a stiff midvein. Similarly, the presence of a stiff midvein in the fern tree leaves rationalizes

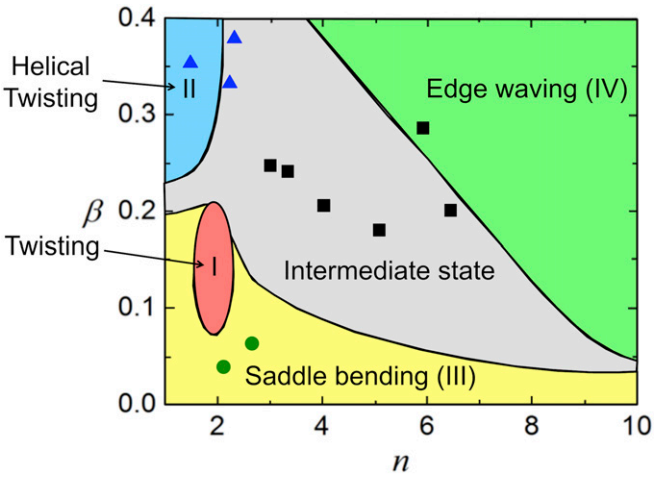

Fig. 4. Phase diagram of morphogenesis of thin plant organs as functions of n and β. Experimental data points are same as those in Fig. 2*B*, where triangles (blue), squares (black), and circles (green) denote leaves with twisting-, edge-waving, and saddle-bending configurations, respectively.

why data points obtained from edge-waving leaves fall within the "intermediate state" region.

Engineering Morphogenesis with Directed Polymerization of Hydrogel. With the foregoing quantitative knowledge of the role of mechanics in plant morphogenesis, we now explore synthetic reproduction of such processes and shapes in engineered systems. We resort to our development on the polyacrylamide (PA) hydrogel (32), in which we control the oxygen concentration to modulate the polymerization of PA hydrogel. As shown in Fig. 5*A*, oxygen diffusion from the surrounding air into the gel solution prevents gelation within the vicinity of liquid–air interface. Polymerization in the region away from the liquid–air interface consumes free monomers and cross-linkers, leading to a concentration gradient of free monomers and cross-linkers, and driving their diffusion from the nongelation region into a polymerized hydrogel network. The continuous polymerization consequently leads to continuous growth of postgelation region (*SI Appendix*, Fig. S5).

We induce differential growth of hydrogel by introducing geometric constraints. An example of such a constraint is a string (e.g., cotton thread) placed parallel to the centerline of the reaction chamber. The thread is relatively inextensible and imposes limited resistance to the out-of-plane bending deformation of the hydrogel sheet. Consequently, local growth of the hydrogel near the thread is inhibited as the edges grow, giving rise to a growth strain profile similar to that given by Eq. **1**. The growth profile can be controlled by adjusting the location and stiffness of the constraining wire within the specimen. When we introduce a pair of cotton threads, separated by a distance of $2\alpha_0 W$, as demonstrated in Fig. 5*A*, the modified growth strain profile can be approximated as

$$\varepsilon_g(y) = \beta \left| \frac{y - \alpha_0 W}{W - \alpha_0 W} \right|^n, \qquad [5]$$

when $|y| \geq \alpha_0 W$. As shown in Fig. 5*B*, increasing the separation distance is essentially equivalent to increasing the value of n. It is difficult to quantify the exact value of the exponent experimentally. However, the configurations of the hydrogel in the presence of the thread suggests that the value is close to $n = 2$ when a single string is placed along the centerline. Fig. 6*A* shows that the hydrogel naturally grows into a twisting configuration (I), and then turns into helical twisting (II) at higher strain level.

Other plant morphogenesis configurations can also be engineered by controlling the degree and location of the constraints. Fig. 6*B* shows that, when placing a pair of constraining threads with a separation distance of $0.68W$, the differential strain mismatch induced by polymerization transforms the hydrogel into a saddle-bending shape (III). Further swelling the hydrogel leads to a configuration with wavy edges (IV).

The unique feature of the present technique is that the continuous polymerization process controlled by oxygen concentration, albeit chemically and mechanistically different, closely mimics the cell growth process in plants controlled by growth factor levels. Fig. 6 demonstrates that, with proper design of constraints, our technique is capable of mimicking morphogenesis of plant leaves and flowers.

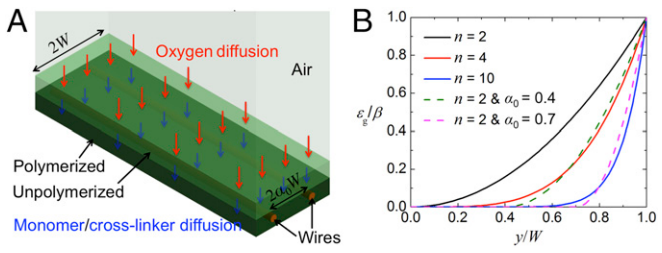

Fig. 5. In vitro reproduction of leaf morphogenesis. (*A*) Schematics of the working principles of the in vitro hydrogel system. (*B*) Manipulation of the growth strain profile in PA hydrogel.

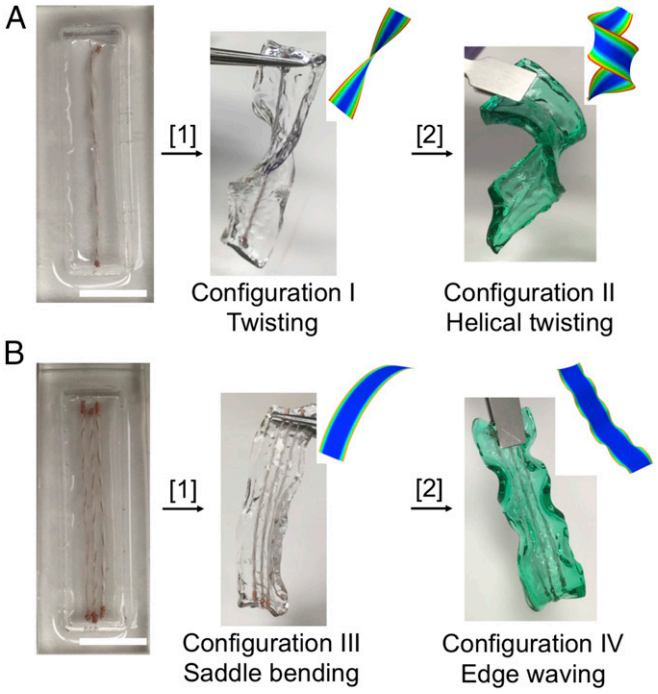

Fig. 6. Reproduction of the four 3D configurations of leaves: (*A*) twisting and helical twisting; (*B*) saddle bending and edge waving. (*Insets*) Contour plots of normalized growth strain profile (ε_g/β) in different configurations: $n = 2$ in *A* and $n = 8$ in *B*. Steps [1] and [2] represent polymerization and hydration, respectively. (Scale bars: 1 cm.)

Discussion

Morphogenesis is achieved by differential growth of tissues in response to controlled distribution of the level of growth factors, and/or different growth rates among different constituent parts (e.g., vascular network vs. leaf lamina). Dictated by genes, the differential growth pattern varies in a plant species- and age-dependent manner. Our study highlights that shape evolution in plant systems is strongly influenced by the mechanics of plant organs—the deformation of tissues to accommodate differential growth, the instabilities that give rise to a cascade of different shapes, and the build-up of strain energy to maintain the shapes. By recourse to quantitative measurements of live leaves, finite-element simulations of differential-growth-induced mechanical deformation of leaf-shaped structures, and experimental models to mimic leaf growth, we elucidate a number of mechanisms underlying plant leaf morphogenesis. More importantly, we have established a general framework to quantify the role of mechanical deformation and geometrical constraints in influencing the evolution of stable shapes commonly found in a number of plant organs. Future work in this area would inevitably call for investigations of a much wider spectrum of plant species as well as considerations of the details of plant leaf shapes, including the cross-sectional shapes and the presence of vascular networks. Besides the in-plane differential growth, the growth across the thickness direction may also vary and play an important role in shaping the leaves (33). A more comprehensive investigation will establish the critical relationship among the spatiotemporal pattern of genetic and molecular factors at molecular level, the

resultant differential growth patterns and 3D shapes at tissue level. Such effort will also require more detailed constitutive models of the mechanics of plant organs than the ones considered in this work.

Besides providing insights into morphogenesis of plant organs in nature, our present work also points to pathways to create bioinspired complex 3D shapes that could find applications in such areas as tissue engineering, flexible electronics, and soft robotics. Biomimetics of the differential growth of thin plant organs in vitro has primarily involved differentially stretching a plastic sheet or rubber, or swelling a patterned hydrogel (4, 12, 34–36). More specifically, material anisotropy has been routinely incorporated to generate twisting and helical-twisting configurations (37–40). Besides the fundamental differences between living tissue growth in nature and hydrogel swelling or stretching in a plastic sheet (32), anisotropic material designs currently invoked in biomimetic systems do not faithfully reproduce the morphogenesis of most biological systems. Our findings point to a more biologically relevant approach to generating twisting and helical-twisting configurations.

Methods

Finite-Element Analysis. The morphogenesis of a growing leaf was simulated using commercial software ABAQUS. We modeled the growing process as an equivalent thermal expansion problem, where a uniform nonzero thermal expansion coefficient was prescribed along the longitudinal direction and a nonuniform temperature field was assigned as an analytical field. The leaf was modeled as an elastic solid discretized by four-node general-purpose shell elements with reduced integration and accounting for finite membrane strains. Before postbuckling analyses, a linear buckling analysis was performed to identify the buckling modes. A linear combination of the first 10 buckling modes was introduced as geometric imperfection into the postbuckling analyses to initiate the out-of-plane buckling. The level of the geometric imperfection was systematically tested to make sure that it was big enough to initiate the out-of-plane deformation but had no influence on the resulting configurations. Constraints were applied to the two short sides (at $x = 0$ and $x = L$ in Fig. 3*A*) to make sure these two edges remain within an y–z plane throughout the simulation (i.e., same displacement along longitudinal direction). The Young modulus and Poisson ratio are $E = 350$ kPa and $v = 0.25$, respectively.

Polymerization of Polyacrylamide Hydrogel. Rectangular reaction chambers were constructed by gently pressing a rectangular polydimethylsiloxane (PDMS) ring onto a glass slide. To prepare the mold for making the PDMS ring, rectangular patterns were cut out of a 6.35-mm-thick acrylic sheet using a laser cutter (Epilog Laser) and then glued onto the bottom surface of a Petri dish using a two-part epoxy (Gorilla Epoxy; Gorilla Glue Inc.). PDMS rings were prepared using a 10:1 weight mixture of base to curing agent (Sylgard 184; Dow Corning). Before being introduced into the reaction chamber, hydrogel solution of 10% acrylamide and 0.1% bis-acrylamide (Amersco) was degassed for 30 min in a vacuum desiccator to completely remove dissolved oxygen, and cotton wires prewetted with hydrogel solution were placed into the reaction chamber as a way to introduce differential growth. Polymerization was then initiated by introducing tetramethylethylenediamine (Teknova) and ammonium persulfate (Promega) into the gel solution with final concentrations of 0.3% and 0.05%, respectively. The gel solution of a desired volume was immediately pipetted into the polymerization chamber with minimal disturbance so as to avoid introducing oxygen. The solution was allowed to react for 1 h before disassembling the reaction chamber to release hydrogel structures.

ACKNOWLEDGMENTS. We thank Richard Piacentini and Jennifer Davit of the Phipps Conservatory and Botanical Gardens in Pittsburgh, PA for providing live plant leaf samples. C.H., D.Q., and K.J.H. gratefully acknowledge financial support from *Eunice Kennedy Shriver* National Institute of Child Health and Human Development Grant R01HD086325 and from CMU. Z.W. acknowledges support from China Scholarship Council – CMU Graduate Fellowship. S.S. acknowledges support from Nanyang Technological University Singapore through the Distinguished University Professorship.

1. Roach P, Shirtcliffe NJ, Newton MI (2008) Progress in superhydrophobic surface development. *Soft Matter* 4:224–240.
2. Wong T-S, et al. (2011) Bioinspired self-repairing slippery surfaces with pressure-stable omniphobicity. *Nature* 477:443–447.
3. Forterre Y, Skotheim JM, Dumais J, Mahadevan L (2005) How the Venus flytrap snaps. *Nature* 433:421–425.
4. Abdullah AM, Nan K, Rogers JA, Hsia KJ (2016) Mismatch strain programmed shape transformation of curved bilayer-flexible support assembly. *Extreme Mech Lett* 7:34–41.
5. Abdullah AM, Braun PV, Hsia KJ (2016) Programmable shape transformation of elastic spherical domes. *Soft Matter* 12:6184–6195.
6. Werner T, Motyka V, Strnad M, Schmülling T (2001) Regulation of plant growth by cytokinin. *Proc Natl Acad Sci USA* 98:10487–10492.
7. Pien S, Wyrzykowska J, McQueen-Mason S, Smart C, Fleming A (2001) Local expression of expansin induces the entire process of leaf development and modifies leaf shape. *Proc Natl Acad Sci USA* 98:11812–11817.
8. Palatnik JF, et al. (2003) Control of leaf morphogenesis by microRNAs. *Nature* 425:257–263.
9. González N, Inzé D (2015) Molecular systems governing leaf growth: From genes to networks. *J Exp Bot* 66:1045–1054.
10. Bilsborough GD, et al. (2011) Model for the regulation of Arabidopsis thaliana leaf margin development. *Proc Natl Acad Sci USA* 108:3424–3429.
11. Kasprzewska A, et al. (2015) Auxin influx importers modulate serration along the leaf margin. *Plant J* 83:705–718.
12. Sharon E, Roman B, Marder M, Shin GS, Swinney HL (2002) Mechanics. Buckling cascades in free sheets. *Nature* 419:579.
13. Gemmer J, Sharon E, Shearman T, Venkataramani SC (2016) Isometric immersions, energy minimization and self-similar buckling in non-Euclidean elastic sheets. *EPL* 114:24003.
14. Li B, Cao Y, Feng X, Gao H (2012) Mechanics of morphological instabilities and surface wrinkling in soft materials : A review. *Soft Matter* 8:5728–5745.
15. Weizbauer R, Peters WS, Schulz B (2011) Geometric constraints and the anatomical interpretation of twisted plant organ phenotypes. *Front Plant Sci* 2:62.
16. Liu Z, Swaddiwudhipong S, Hong W (2013) Pattern formation in plants via instability theory of hydrogels. *Soft Matter* 9:577–587.
17. van Doorn WG, Kamdee C (2014) Flower opening and closure: An update. *J Exp Bot* 65:5749–5757.
18. Liang H, Mahadevan L (2009) The shape of a long leaf. *Proc Natl Acad Sci USA* 106: 22049–22054.
19. Liang H, Mahadevan L (2011) Growth, geometry, and mechanics of a blooming lily. *Proc Natl Acad Sci USA* 108:5516–5521.
20. Smyth DR (2016) Helical growth in plant organs: Mechanisms and significance. *Development* 143:3272–3282.
21. Ishida T, Kaneko Y, Iwano M, Hashimoto T (2007) Helical microtubule arrays in a collection of twisting tubulin mutants of Arabidopsis thaliana. *Proc Natl Acad Sci USA* 104:8544–8549.
22. Wada H (2012) Hierarchical helical order in the twisted growth of plant organs. *Phys Rev Lett* 109:128104.
23. Saffer AM, Carpita NC, Irish VF (2017) Rhamnose-containing cell wall polymers suppress helical plant growth independently of microtubule orientation. *Curr Biol* 27: 2248–2259.e4.
24. Huang X, Yuan H, Hsia KJ, Zhang S (2010) Coordinated buckling of thick multi-walled carbon nanotubes under uniaxial compression. *Nano Res* 3:32–42.
25. Hu H, Huang C, Liu XH, Hsia KJ (2016) Thin film wrinkling by strain mismatch on 3D surfaces. *Extreme Mech Lett* 8:107–113.
26. Panat R, Hsia KJ (2004) Experimental investigation of the bond-coat rumpling instability under isothermal and cyclic thermal histories in thermal barrier systems. *Proc R Soc* 460:1957–1979.
27. Saito T, Soga K, Hoson T, Terashima I (2006) The bulk elastic modulus and the reversible properties of cell walls in developing Quercus leaves. *Plant Cell Physiol* 47: 715–725.
28. Hayot CM, Forouzesh E, Goel A, Avramova Z, Turner JA (2012) Viscoelastic properties of cell walls of single living plant cells determined by dynamic nanoindentation. *J Exp Bot* 63:2525–2540.
29. Lalonde S, Tegeder M, Throne-Holst M, Frommer WB, Patrick JW (2003) Phloem loading and unloading of sugars and amino acids. *Plant Cell Environ* 26:37–56.
30. Kierzkowski D, et al. (2012) Elastic domains regulate growth and organogenesis in the plant shoot apical meristem. *Science* 335:1096–1099.
31. Sampathkumar A, Yan A, Krupinski P, Meyerowitz EM (2014) Physical forces regulate plant development and morphogenesis. *Curr Biol* 24:R475–R483.
32. Huang C, Quinn D, Suresh S, Hsia KJ (2018) Controlled molecular self-assembly of complex three-dimensional structures in soft materials. *Proc Natl Acad Sci USA* 115: 70–74.
33. Rebocho AB, Southam P, Kennaway JR, Bangham JA, Coen E (2017) Generation of shape complexity through tissue conflict resolution. *eLife* 6:1–45.
34. Tallinen T, Chung JY, Biggins JS, Mahadevan L (2014) Gyrification from constrained cortical expansion. *Proc Natl Acad Sci USA* 111:12667–12672.
35. Mora T, Boudaoud A (2006) Buckling of swelling gels. *Eur Phys J E Soft Matter* 20:119–124.
36. Motala MJ, et al. (2015) Programming matter through strain. *Extreme Mech Lett* 3:8–16.
37. Gladman AS, Matsumoto EA, Nuzzo RG, Mahadevan L, Lewis JA (2016) Biomimetic 4D printing. *Nat Mater* 15:413–418.
38. Armon S, Efrati E, Kupferman R, Sharon E (2011) Geometry and mechanics in the opening of chiral seed pods. *Science* 333:1726–1730.
39. Wu ZL, et al. (2013) Three-dimensional shape transformations of hydrogel sheets induced by small-scale modulation of internal stresses. *Nat Commun* 4:1586–1587.
40. Oda R, Huc I, Schmutz M, Candau SJ, MacKintosh FC (1999) Tuning bilayer twist using chiral counterions. *Nature* 399:566–569.